

Nonseparable Gaussian Stochastic Process: A Unified View and Computational Strategy

Mengyang Gu and Yanxun Xu

Department of Applied Mathematics and Statistics, Johns Hopkins University, Baltimore, MD

Abstract

Gaussian stochastic process (GaSP) has been widely used as a prior over functions due to its flexibility and tractability in modeling. However, the computational cost in evaluating the likelihood is $O(n^3)$, where n is the number of observed points in the process, as it requires to invert the covariance matrix. This bottleneck prevents GaSP being widely used in large-scale data. We propose a general class of nonseparable GaSP models for multiple functional observations with a fast and exact algorithm, in which the computation is linear ($O(n)$) and exact, requiring no approximation to compute the likelihood. We show that the commonly used linear regression and separable models are both special cases of the proposed nonseparable GaSP model. The advantages of our nonseparable GaSP model are illustrated in an epigenetic application in which the genome-wide DNA methylation levels are predicted.

KEY WORDS: Exact computation, Fast algorithm, Methylation levels imputation, Multiple functional data, Stochastic differential equations

1 Introduction

The increasing demands to analyze high dimensional data with complex structure have facilitated the development of novel statistical models for functional data, in which the outcomes can be interpreted as samples of random functions. Time series, longitudinal, and spatial data are some typical examples of function data. One common feature among functional data is that, often, a simple conditional model does not appropriately explain the correlations between the outcomes that are close in the inputs of the function. A model that expresses the inputs and outcomes jointly is preferred, when the mapping from the functional inputs to the associated outcomes is modeled as a stochastic process, and the correlations between nearby inputs are captured through a covariance matrix. One natural choice of such stochastic process is the Gaussian stochastic process (GaSP), which has been widely used in many applications (Sacks et al., 1989; Bayarri et al., 2009; Gelfand et al., 2010; Xu and Ji, 2014).

GaSP models have also been popular in analyzing functional data with multiple functional outcomes (Álvarez et al., 2011; Banerjee et al., 2014), in which independent GaSP models are generally built separately for each outcome for simplicity. A more sophisticated approach is to define a separable GaSP model, where the correlations between functions and between inputs are modeled separately using a matrix normal distribution (Conti and O’Hagan, 2010). Other approaches include estimating a basis function, such as using principal components (Higdon et al., 2008) or wavelets (Bayarri et al., 2007), with the weights of the basis function modeled as an independent Gaussian process to create correlation structure over the input space. This construction results in *nonseparable* covariance structures, meaning that the covariance matrix cannot be decomposed as a Kronecker product of two small covariance matrices. More general nonseparable covariance structures include process convolution by convolving the base GaSPs with some smooth kernel functions (Higdon et al., 2002; Alvarez

and Lawrence, 2011).

For large-scale data, a GaSP model is sometimes too computationally expensive: the evaluation of the likelihood has computational complexity $O(n^3)$, where n is the number of observed data points. Specifically, evaluating the likelihood requires the inverse of the covariance matrix, which is typically a dense $n \times n$ matrix. Many approximation methods have been proposed, including low rank approximation (Cressie and Johannesson, 2008; Banerjee et al., 2008), covariance tapering and compactly support covariance (Furrer et al., 2012; Kaufman et al., 2008, 2011), use of Gaussian Markov random field representations (Rue et al., 2009; Lindgren et al., 2011), and likelihood approximation (Eidsvik et al., 2013), etc. See, for example, Chapter 3 of Sun et al. (2012) for an overview.

In this work, we propose a general framework that unifies the linear regression, separable and nonseparable GaSP models. Moreover, we develop an ultra-fast inference method that computes the exact likelihood without approximation with $O(n)$ computational operations, when using a class of commonly-used covariance functions. Instead of computing the inverse of the covariance matrix directly, the evaluation of the likelihood is significantly simplified by the connection between the Gaussian random field and Gaussian Markov random field. This enables the use of the GaSP model to large-scale data.

The rest of the paper is organized as follows. We first introduce a motivating scientific problem—the imputation of DNA methylation levels—in the following subsection. In Section 2, we approach this problem by modeling multiple functional data using the linear regression and separable GaSP models. In Section 3, we further introduce a class of nonseparable GaSP models that unifies the regression and separable models. In Section 4, we discuss the computational strategy for this class of nonseparable GaSP models, for which the computation scales linearly in the number of inputs. Numerical examples and comparisons to alternative methods are provided in Section 5. We conclude the paper with discussion and future extensions in Section 6.

1.1 Motivating study: interpolating DNA methylation levels in the human genome

Our motivating study is to impute DNA methylation levels at CpG sites across the human genome. DNA methylation is an epigenetic modification of DNA, playing important roles in DNA replication, gene transcription, aging, and cancer evolution (Das and Singal, 2004; Scarano et al., 2005). Methylation levels are quantified at every genomic CpG site, a region of DNA where a cytosine (C) nucleotide is followed by a guanine (G) nucleotide in the linear sequence of bases along its 5' to 3' direction. Single-site DNA methylation level can be quantified by whole-genome bisulfite sequencing (WGBS), in which approximately 26 million CpG sites in the human genome are evaluated for whether they are methylated or not. However, WGBS is expensive and hard to examine in certain genomic regions. This motivates alternative methylation assay technologies, such as Illumina HumanMethylation450 BeadChip that measures DNA methylation levels at approximately 482,000 CpG sites (less than 2% of the total number of CpG sites).

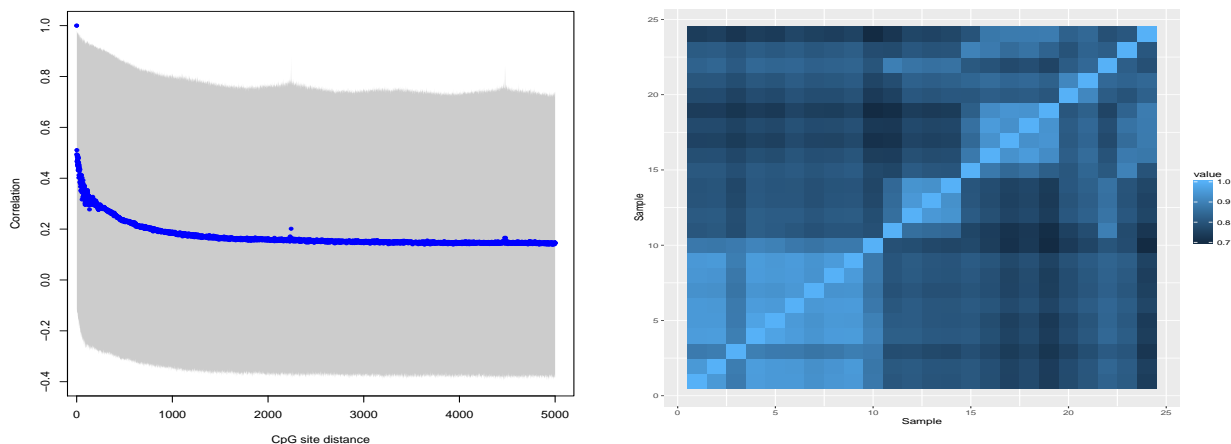


Figure 1: Empirical correlation of methylation levels across sites (left panel) and across samples (right panel). The blue dots in the left panel are the average correlation of the methylation levels between two CpG sites at a given CpG distance not larger than 5000 and the shaded area is the empirical 95% confidence interval. The number of samples is 24 and each sample has 1.6 million methylation levels.

The goal of this study is to impute DNA methylation levels at the CpG sites that are observed in the WGBS samples but unobserved in the 450K data by exploiting the correlations in methylation levels among the full set of CpG sites in the WGBS samples. The empirical correlation of methylations levels with distance smaller than 5 kilobases in the WGBS samples is shown in the left panel of Figure 1. For each integer distance, we calculate the empirical correlation of every possible pair with this distance. The blue curve is the average empirical correlation and the shaded area is the empirical 95% confidence interval. The methylation levels at nearby CpG sites are correlated to each other on average and the correlation gradually decays as the distance between the two CpG sites increases. Such phenomenon is called co-methylation and has been observed in previous studies (Eckhardt et al., 2006; Zhang et al., 2015). Large heterogeneity across sites is also found by the wide 95% confidence interval. Furthermore, as shown in the right panel of Figure 1, methylation levels for each CpG site across samples are well correlated for biological reasons. Since methylation plays important roles in suppressing gene expression levels, they are tightly regulated in cells and variability of such regulations is associated with disease risk (Das and Singal, 2004). Understanding the correlation patterns in methylations levels is thus meaningful for reducing the risk of diseases. These empirical findings motivate us to develop a statistical model to exploit the correlations of methylation levels across the genome sites and across different samples for the goal of imputation.

2 Modeling multiple functional data

Let $y_i(s_j)$ be the methylation level of the i^{th} sample at the j^{th} CpG site, recording the proportion of probes for a single CpG site that is methylated, for $i = 1, \dots, K, j = 1, \dots, N$. Define two groups of sites, $\mathbf{s}^{\mathcal{D}} = \{s_1^{\mathcal{D}}, \dots, s_n^{\mathcal{D}}\}$ and $\mathbf{s}^* = \{s_1^*, \dots, s_{n^*}^*\}$, where the methylation levels of $\mathbf{s}^{\mathcal{D}}$ are observed for all K samples and the methylation levels of $\mathbf{s}^* = \{s_1^*, \dots, s_{n^*}^*\}$

are only available for the first k samples but not available for the last k^* samples. The total number of samples is $K = k + k^*$ and the total number of CpG sites is $N = n + n^*$.

For the first k samples, methylation levels are measured at all CpG sites, meaning that we observe $\mathbf{y}(\mathbf{s}^{\mathcal{D}})_{[k \times n]}$ and $\mathbf{y}(\mathbf{s}^*)_{[k \times n^*]}$. However, for the remaining k^* samples, the methylation levels are only observed at a small subset of CpG sites, denoted as $\mathbf{y}^*(\mathbf{s}^{\mathcal{D}})_{[k^* \times n]}$. The methylation levels at the remaining CpG sites ($\mathbf{y}^*(\mathbf{s}^*)_{[k^* \times n^*]}$) of these samples are unknown. Our goal, then, is to interpolate the unobserved methylation levels of these k^* samples using their observed methylation values at n CpG sites and the full methylation values from the other k samples. In other words, we seek the predictive distribution of $\mathbf{y}^*(\mathbf{s}^*)$ conditional on $\mathbf{y}(\mathbf{s}^{\mathcal{D}})$, $\mathbf{y}(\mathbf{s}^*)$ and $\mathbf{y}^*(\mathbf{s}^{\mathcal{D}})$.

The imputation of methylation levels across the whole genome is computationally challenging due to the large number of CpG sites. In the full WGBS data set, there are about 2.8×10^7 CpG sites; even in the smaller Methylation450K data there are roughly 4.5×10^5 CpG sites, creating computational challenges. In contrast, the number of samples we are working with is relatively small: $k = 24$ samples in the WGBS data and $k^* = 100$ samples in the Methylation450K data. The key advantage of our method is that the computation required for imputation scales linearly in terms of the number of CpG sites.

In the following, we start with the linear regression model that was used for methylation level imputation (Zhang et al., 2015), and then we introduce the separable model. In Section 3, we show these models are special cases of the nonseparable GaSP model.

2.1 Linear regression strategies

Assuming that the samples are independent to each other, a simple model is to apply the linear regression separately for each CpG site s_j , $j = 1, \dots, N$, as follows,

$$y_i(s_j) = \mathbf{H}_i(s_j)\boldsymbol{\beta}_j + \epsilon_{ij}, \quad i = 1, \dots, K, \quad (1)$$

where $\mathbf{H}_i(s_j)$ are the covariates for the j^{th} CpG site of the i^{th} sample and $\epsilon_{ij} \sim N(0, \sigma_{0j}^2)$ is an independent mean-zero Gaussian noise. In Zhang et al. (2015), 124 site-specific features, including methylation levels at nearby CpG sites, are used as covariates. This approach assumes that methylation levels are independent across samples at every CpG site. However, methylation levels of different samples at a CpG site are generally correlated, as shown in Figure 1. We later will show that exploiting the correlation between samples leads to drastic improvement in imputation.

Alternatively, one can assume a regression model that exploits the correlations across different samples,

$$y_i(s_j) = \mathbf{H}_i(s_j)\boldsymbol{\beta}_i + \epsilon_{ij}, \quad j = 1, \dots, N, \quad (2)$$

with $\epsilon_{ij} \sim N(0, \sigma_{i0}^2)$. With this specification, each site is treated independently. When the methylation levels were first normalized to have a zero mean and let $\mathbf{H}_i(s_j) = (y_1(s_j), \dots, y_k(s_j))$, meaning only the methylation levels of the k samples with full observations are used as covariates, the model for $\mathbf{s}^{\mathcal{D}}$ can be expressed as follows

$$\mathbf{y}_i^*(\mathbf{s}^{\mathcal{D}})^T = \mathbf{y}(\mathbf{s}^{\mathcal{D}})^T \boldsymbol{\beta}_i + \boldsymbol{\epsilon}_i,$$

where $\mathbf{y}_i^*(\mathbf{s}^{\mathcal{D}})$ is the i^{th} row of $\mathbf{y}^*(\mathbf{s}^{\mathcal{D}})$ and $\boldsymbol{\epsilon}_i \sim N(0, \sigma_{i0}^2 \mathbf{I}_n)$. The least squares (LS) estimator of $\boldsymbol{\beta}_i$ is then

$$\hat{\boldsymbol{\beta}}_i = \{\mathbf{y}(\mathbf{s}^{\mathcal{D}})\mathbf{y}(\mathbf{s}^{\mathcal{D}})^T\}^{-1} \mathbf{y}(\mathbf{s}^{\mathcal{D}})\mathbf{y}_i^*(\mathbf{s}^{\mathcal{D}})^T,$$

where $\mathbf{y}_i^*(\mathbf{s}^{\mathcal{D}}) = (y_i^*(\mathbf{s}_1^{\mathcal{D}}), \dots, y_i^*(\mathbf{s}_n^{\mathcal{D}}))$ being the i^{th} row of $\mathbf{y}^*(\mathbf{s}^{\mathcal{D}})$. The predictive mean of the methylation level of the i^{th} sample at the j^{th} unexamined site is

$$\mathbb{E}[\mathbf{y}_i^*(s_j^*) \mid \mathbf{y}(\mathbf{s}^{\mathcal{D}}), \mathbf{y}^*(\mathbf{s}^{\mathcal{D}}), \mathbf{y}(\mathbf{s}^*)] = \mathbf{H}_i(s_j^*)\hat{\boldsymbol{\beta}}_i = \mathbf{y}(s_j^*)^T \{\mathbf{y}(\mathbf{s}^{\mathcal{D}})\mathbf{y}(\mathbf{s}^{\mathcal{D}})^T\}^{-1} \mathbf{y}(\mathbf{s}^{\mathcal{D}})\mathbf{y}_i^*(\mathbf{s}^{\mathcal{D}})^T, \quad (3)$$

with $\mathbf{y}(s_j^*) = (y_1(s_j^*), \dots, y_k(s_j^*))^T$ being the j^{th} column of $\mathbf{y}(\mathbf{s}^*)$, for $i = 1, \dots, k^*$, $j = 1, \dots, n^*$.

Only the methylation levels of the first k samples are used as the regressors for illustrative purposes, but the intercept and additional features can be incorporated into the covariates, as discussed in Section 3.2. We later show that equation (3) is the predictive mean of the nonseparable model with the certain choice of parameters.

2.2 Separable model

Denote

$$\mathbf{Y} = \begin{pmatrix} \mathbf{y}(\mathbf{s}^{\mathcal{D}}) & \mathbf{y}(\mathbf{s}^*) \\ \mathbf{y}^*(\mathbf{s}^{\mathcal{D}}) & \mathbf{y}^*(\mathbf{s}^*) \end{pmatrix}.$$

Compared to the regression models, the following joint model is sometimes preferred

$$\mathbf{Y} = \mathbf{Z} + \boldsymbol{\epsilon}_0, \tag{4}$$

where $\boldsymbol{\epsilon}_0$ is a zero-mean independent noise and \mathbf{Z} is a $K \times N$ random matrix modeled from a matrix-variate normal distribution (Wang and West, 2009), $\mathbf{Z} \sim N_{K,N}(\boldsymbol{\mu}, \boldsymbol{\Sigma}, \boldsymbol{\Lambda})$, with a $K \times N$ mean matrix $\boldsymbol{\mu}$, a $K \times K$ row covariance matrix $\boldsymbol{\Sigma}$, and an $N \times N$ column correlation matrix $\boldsymbol{\Lambda}$. The density of \mathbf{Z} is

$$p(\mathbf{Z}|\boldsymbol{\mu}, \boldsymbol{\Sigma}, \boldsymbol{\Lambda}) = \frac{\exp(-\frac{1}{2}\text{tr}[\boldsymbol{\Sigma}^{-1}(\mathbf{Z} - \boldsymbol{\mu})^T \boldsymbol{\Lambda}^{-1}(\mathbf{Z} - \boldsymbol{\mu})])}{(2\pi)^{NK/2} |\boldsymbol{\Sigma}|^{N/2} |\boldsymbol{\Lambda}|^{K/2}}.$$

We call model (4) *the separable model*, as the correlations across samples and across sites are expressed separately by $\boldsymbol{\Sigma}$ and $\boldsymbol{\Lambda}$ respectively. The correlations across samples are modeled by $\boldsymbol{\Sigma}$, partitioned into four blocks $\boldsymbol{\Sigma} = \begin{pmatrix} \boldsymbol{\Sigma}_{00} & \boldsymbol{\Sigma}_{0*} \\ \boldsymbol{\Sigma}_{*0} & \boldsymbol{\Sigma}_{**} \end{pmatrix}$, where $\boldsymbol{\Sigma}_{00}$, $\boldsymbol{\Sigma}_{**}$ and $\boldsymbol{\Sigma}_{0*}$ are the covariances of the first k samples, the last k^* samples, and between the first k and the last k^* samples, respectively. As shown in Figure 1, the methylation levels at nearby CpG sites are correlated and decay as the genomic distance increases. This motivates us to

model $\mathbf{\Lambda}$ via a kernel function. One of the popular choice is the Matérn kernel, which has the following form

$$c(d) = \frac{1}{2^{\nu-1}\Gamma(\nu)} \left(\frac{d}{\gamma}\right)^{\nu} \mathcal{K}_{\nu}\left(\frac{d}{\gamma}\right), \quad (5)$$

where $\Gamma(\cdot)$ is the gamma function and $\mathcal{K}_{\nu}(\cdot)$ is the modified Bessel function of the second kind with a roughness parameter ν , a range parameter γ and $d = |s_a - s_b|$ for any $s_a, s_b \in \mathcal{S}$. The roughness parameter of the Matérn kernel controls how smooth the stochastic process is. When $\nu = (2m + 1)/2$ with $m \in \mathbb{N}$, the GaSP with a Matérn kernel is m^{th} sample path differentiable and the Matérn kernel has a closed form expression in these scenarios. For instance, the exponential kernel is equivalent to the Matérn kernel with $\nu = 1/2$ and the Gaussian kernel is the Matérn kernel with $\nu \rightarrow +\infty$. The flexibility of the Matérn kernel makes it widely applicable for modeling spatially correlated data (Gelfand et al. (2010)).

The most challenging part of the separable model is the computation when n is large. As discussed in Section 1, evaluating the exact likelihood involves the inversion of the covariance matrix, which requires $O(n^3)$ computational operations. Additional computational advantages of using the Matérn kernel will be introduced in Section 4. Besides, the separable model assumes that the correlation matrix between sites is shared for each sample, which is sometimes too restrictive in practice. To address these challenges and limitations, we will introduce a nonseparable model with the following features:

- Gaussian stochastic processes with the Matérn covariance are used to model correlation across sites, which is allowed to vary across samples;
- Only $O(n)$ and $O(N)$ computational operations are needed for computing the likelihood exactly and for predicting unobserved methylation levels without approximation, respectively;
- The imputations by the regression and by the separable model correspond to special cases of this nonseparable model.

3 Nonseparable GaSP model

In this section, we develop a class of nonseparable GaSP models. This class of model has been proposed for modeling multivariate spatially correlated data (see e.g. Gelfand et al. (2004); Banerjee et al. (2008)) and for calibrating a computer model with multiple outcomes (Higdon et al. (2008)). We make several extensions. First and foremost, we introduce a computationally feasible way for the nonseparable GaSP model to the large-scale problems with inputs up to a million without approximating the likelihood function. Furthermore, we construct a flexible way to incorporate the correlations across samples and across sites for imputation on methylation levels. Lastly, the connection between this nonseparable model and the previously introduced regression model and the separable GaSP model is established. The proofs of lemmas are given in Appendix A.

We start with the model,

$$\mathbf{Y}(s) = \mathbf{A}\mathbf{v}(s) + \boldsymbol{\epsilon}_0, \quad (6)$$

for every site $s \in \mathcal{S}$, where $\boldsymbol{\epsilon}_0 \sim N(\mathbf{0}, \sigma_0^2 \mathbf{I}_K)$, $\mathbf{A} = (\mathbf{a}_1; \dots; \mathbf{a}_K)$ is a $K \times K$ matrix with \mathbf{a}_i being the i^{th} basis function ($K \times 1$ vector) specified later, and $\mathbf{v}(\cdot) = (v_1(\cdot), \dots, v_K(\cdot))^T$. Each weight function $v_i(\cdot)$ is independently modeled as a zero mean Gaussian stochastic process (GaSP)

$$v_i(\cdot) \sim \text{GaSP}(0, \sigma_i^2 c_i(\cdot, \cdot)), \quad (7)$$

where σ_i^2 is an unknown variance parameter, $c_i(s_a, s_b)$ being the correlation between sites specified as in (5), with a prespecified ν_i and an unknown range parameter γ_i , for $i = 1, \dots, K$. For the purpose of illustration, we do not model the mean function at the current stage, but such issue will be addressed in Section 3.2.

The following remark states the separable model defined in (4) is a special case of the

nonseparable model in (6).

Remark 1. *If $\boldsymbol{\mu} = \mathbf{0}$, the separable model defined in (4) is equivalent to the nonseparable GaSP model in (6) if*

(i.) \mathbf{A} is chosen such that $\boldsymbol{\Sigma} = \mathbf{A}\mathbf{A}^T$.

(ii.) For different i , the covariance function of $v_i(\cdot)$ has the unit variance and shares the same γ_i , $i = 1, \dots, K$.

Denote $\mathbf{Y}(\mathbf{s}^{\mathcal{D}}) = (\mathbf{y}(\mathbf{s}^{\mathcal{D}})^T; \mathbf{y}^*(\mathbf{s}^{\mathcal{D}})^T)^T$. Following Higdon et al. (2008), we apply the singular value decomposition (SVD) to $\mathbf{Y}(\mathbf{s}^{\mathcal{D}}) = \mathbf{U}\mathbf{D}\mathbf{V}$ and estimate \mathbf{A} as $\mathbf{A} = \mathbf{U}\mathbf{D}/\sqrt{n}$, for the following reasons. First of all, the computational order of estimating \mathbf{A} is linear to n , which is essential when n is at the size of 10^6 . Secondly, we have $\mathbf{a}_i^T \mathbf{a}_j = 0$ if $i \neq j$, and hence $\mathbf{A}^T \mathbf{A}$ is a diagonal matrix, which substantially simplifies the computation of the likelihood. Moreover, $\mathbf{A}\mathbf{A}^T = \mathbf{Y}(\mathbf{s}^{\mathcal{D}})\mathbf{Y}(\mathbf{s}^{\mathcal{D}})^T/n$, unifying the linear regression model under the framework of the nonseparable model shown later in Remark 2.

One can marginalize out the $K \times n$ weight matrix $\mathbf{v}(\mathbf{s}^{\mathcal{D}})$ explicitly for computing the likelihood. We first vectorize outputs $\mathbf{Y}_v(\mathbf{s}^{\mathcal{D}}) := \text{vec}(\mathbf{Y}(\mathbf{s}^{\mathcal{D}}))$ and weight matrix $\mathbf{v}_v(\mathbf{s}^{\mathcal{D}}) := \text{vec}(\mathbf{v}(\mathbf{s}^{\mathcal{D}})^T)$, both of which are Kn -dimensional vectors. Define a $Kn \times Kn$ matrix $\mathbf{A}_v := [\mathbf{I}_n \otimes \mathbf{a}_1; \dots; \mathbf{I}_n \otimes \mathbf{a}_K]$. By simple algebra, model (6) can be written as,

$$\mathbf{Y}_v(\mathbf{s}^{\mathcal{D}}) = \mathbf{A}_v \mathbf{v}_v(\mathbf{s}^{\mathcal{D}}) + \boldsymbol{\epsilon}_{0v}, \quad (8)$$

where $\boldsymbol{\epsilon}_{0v} \sim N(0, \sigma_0^2 \mathbf{I}_{nK})$ and $\mathbf{v}_v(\mathbf{s}^{\mathcal{D}}) \mid \sigma_1^2, \dots, \sigma_K^2, \mathbf{R}_1, \dots, \mathbf{R}_K \sim MN(\mathbf{0}, \boldsymbol{\Sigma}_v)$, with the (l, m) entry of the \mathbf{R}_i being $c_i(s_l^{\mathcal{D}}, s_m^{\mathcal{D}})$. Here $\boldsymbol{\Sigma}_v = \text{blkdiag}(\sigma_1^2 \mathbf{R}_1; \dots; \sigma_K^2 \mathbf{R}_K)$, where $\text{blkdiag}(\cdot)$ means the block diagonal matrix between sites, and \mathbf{R}_i is the i^{th} correlation matrix, $i = 1, \dots, K$. As shown in Higdon et al. (2008), directly marginalizing out $\mathbf{v}_v(\mathbf{s}^{\mathcal{D}})$ leads to the

sampling model for $\mathbf{Y}_v(\mathbf{s}^{\mathcal{D}})$ as follows

$$\mathbf{Y}_v(\mathbf{s}^{\mathcal{D}}) \mid \sigma_0^2, \sigma_1^2, \dots, \sigma_K^2, \mathbf{R}_1, \dots, \mathbf{R}_K \sim \mathcal{MN}(\mathbf{0}, \mathbf{A}_v \boldsymbol{\Sigma}_v \mathbf{A}_v^T + \sigma_0^2 \mathbf{I}_{Kn}). \quad (9)$$

The straightforward computation of the likelihood in the above sampling model requires to evaluate the inverse of a $Kn \times Kn$ covariance matrix $\mathbf{A}_v \boldsymbol{\Sigma}_v \mathbf{A}_v^T + \sigma_0^2 \mathbf{I}_{Kn}$, which is computationally infeasible. We have the following lemma to ease the computational challenge.

Lemma 1. *Assume $\mathbf{A} = \mathbf{U}\mathbf{D}/\sqrt{n}$ and $\mathbf{Y}(\mathbf{s}^{\mathcal{D}}) = \mathbf{U}\mathbf{D}\mathbf{V}$ as the SVD decomposition. After integrating out $\mathbf{v}(\mathbf{s}^{\mathcal{D}})$, the marginal likelihood of $\mathbf{Y}(\mathbf{s}^{\mathcal{D}})$ in model (6) follows a product of K independent multivariate normal distributions,*

$$p(\mathbf{Y}(\mathbf{s}^{\mathcal{D}}) \mid \sigma_0^2, \sigma_1^2, \dots, \sigma_K^2, \mathbf{R}_1, \dots, \mathbf{R}_K) = |\mathbf{A}_v^T \mathbf{A}_v|^{-1/2} \prod_{i=1}^K p_{MN}(\hat{\mathbf{v}}_i(\mathbf{s}^{\mathcal{D}}); \mathbf{0}, \sigma_i^2 \mathbf{R}_i + \sigma_0^2 (\mathbf{a}_i^T \mathbf{a}_i)^{-1} \mathbf{I}_n), \quad (10)$$

where $p_{MN}(\cdot; \boldsymbol{\mu}, \boldsymbol{\Sigma})$ denotes the multivariate normal density with mean $\boldsymbol{\mu}$ and covariance $\boldsymbol{\Sigma}$, $\hat{\mathbf{v}}_i(\mathbf{s}^{\mathcal{D}})$ is the transpose of the i^{th} row of $\hat{\mathbf{v}}(\mathbf{s}^{\mathcal{D}}) = (\mathbf{A}^T \mathbf{A})^{-1} \mathbf{A}^T \mathbf{Y}(\mathbf{s}^{\mathcal{D}})$.

Lemma 1 states that the marginal likelihood by model (6) can be written as a product of K multivariate normal densities, which simplifies the computation. In particular, instead of computing the multivariate normal densities with a $Kn \times Kn$ covariance matrix, one can evaluate the densities by K independent multivariate normal distributions, each of which has an $n \times n$ covariance matrix. The direct computation of the inverse of an $n \times n$ covariance matrix, however, is still very hard in general, when n is at the size of 10^6 . An efficient algorithm that computes the exact likelihood without approximation will be provided in Section 4.

The goal of imputation is to find the predictive distribution at an unexamined site s_j^* conditioning on the available data. Denote $\mathbf{Y}(s_j^*) = (\mathbf{y}(s_j^*)^T; \mathbf{y}^*(s_j^*)^T)^T$, where $\mathbf{y}(s_j^*)$ and $\mathbf{y}^*(s_j^*)$ are the j^{th} column of $\mathbf{y}(\mathbf{s}^*)$ and $\mathbf{y}^*(\mathbf{s}^*)$ respectively. We have the following lemma.

Lemma 2. *We assume the same conditions in Lemma 1.*

1. *For every s_j^* , one has*

$$\mathbf{Y}(s_j^*) \mid \mathbf{Y}(\mathcal{S}), \sigma_{0:K}^2, \gamma_{1:K} \sim MN \left(\hat{\boldsymbol{\mu}}(s_j^*), \hat{\boldsymbol{\Sigma}}(s_j^*) \right).$$

Here $\hat{\boldsymbol{\mu}}(s_j^*) = \mathbf{A}\hat{\mathbf{v}}^*(s_j^*)$ and $\hat{\boldsymbol{\Sigma}}(s_j^*) = \mathbf{A}\mathbf{D}^*(s_j^*)\mathbf{A}^T + \sigma_0^2\mathbf{I}_K$, where $\hat{\mathbf{v}}^*(s_j^*) = (\hat{v}_1^*(s_j^*), \dots, \hat{v}_K^*(s_j^*))^T$ with $\hat{v}_i^*(s_j^*) = \mathbf{r}_i^T(s_j^*)(\mathbf{R}_i + \frac{\sigma_0^2(\mathbf{a}_i^T \mathbf{a}_i)^{-1}}{\sigma_i^2} \mathbf{I}_n)^{-1} \hat{\mathbf{v}}_i(s_j^*)$ and $\hat{\mathbf{v}}_i(s_j^*)$ being the transpose of the i^{th} row of $\hat{\mathbf{v}}(s_j^*)$, $\mathbf{r}_i(s_j^*) = (c_i(s_j^*, s_1^*), \dots, c_i(s_j^*, s_n^*))^T$, $\mathbf{D}^*(s_j^*)$ is a $K \times K$ diagonal matrix with $\sigma_i^2 c_i^*(s_j^*)$ as the i^{th} entry in the diagonal terms and $c_i^*(s_j^*) = c_i(s_j^*, s_j^*) - \mathbf{r}_i^T(s_j^*)(\mathbf{R}_i + \frac{\sigma_0^2(\mathbf{a}_i^T \mathbf{a}_i)^{-1}}{\sigma_i^2} \mathbf{I}_n)^{-1} \mathbf{r}_i(s_j^*)$.

2. *Denote the partition $\hat{\boldsymbol{\mu}}(s_j^*) = (\hat{\boldsymbol{\mu}}_0^T(s_j^*), \hat{\boldsymbol{\mu}}_*^T(s_j^*))^T$ and $\hat{\boldsymbol{\Sigma}}(s_j^*) = \begin{pmatrix} \hat{\boldsymbol{\Sigma}}_{00}(s_j^*) & \hat{\boldsymbol{\Sigma}}_{0*}(s_j^*) \\ \hat{\boldsymbol{\Sigma}}_{*0}(s_j^*) & \hat{\boldsymbol{\Sigma}}_{**}(s_j^*) \end{pmatrix}$.*

For every s_j^ , the predictive distribution of the unobserved $\mathbf{y}^*(s_j^*)$ follows*

$$\mathbf{y}^*(s_j^*) \mid \mathbf{y}(\mathcal{S}), \mathbf{y}(s_j^*), \mathbf{y}^*(\mathcal{S}), \sigma_{0:K}^2, \gamma_{1:K} \sim MN \left(\hat{\boldsymbol{\mu}}_{*|0}(s_j^*), \hat{\boldsymbol{\Sigma}}_{*|0}(s_j^*) \right),$$

where $\hat{\boldsymbol{\mu}}_{*|0}(s_j^*) = \hat{\boldsymbol{\mu}}_*(s_j^*) + \hat{\boldsymbol{\Sigma}}_{*0}(s_j^*) \hat{\boldsymbol{\Sigma}}_{00}^{-1}(s_j^*) (\mathbf{y}(s_j^*) - \hat{\boldsymbol{\mu}}_0(s_j^*))$ and $\hat{\boldsymbol{\Sigma}}_{*|0}(s_j^*) = \hat{\boldsymbol{\Sigma}}_{**}(s_j^*) - \hat{\boldsymbol{\Sigma}}_{*0}(s_j^*) \hat{\boldsymbol{\Sigma}}_{00}^{-1}(s_j^*) \hat{\boldsymbol{\Sigma}}_{0*}(s_j^*)$.

In the methylation levels imputation study, $\hat{\boldsymbol{\mu}}_{*|0}(s_j^*)$ can be used as predictions for $\mathbf{y}^*(s_j^*)$ for any site s_j^* , by properly conditional on all observations. The inference of parameters $\sigma_{0:K}^2$ and $\gamma_{1:K}$ along with the computation strategy will be discussed in Section 4. The following remark establishes the connection between the linear regression and nonseparable GaSP model.

Remark 2. *The predictive mean under the linear regression model in (3) is identical to the predictive mean $\hat{\boldsymbol{\mu}}_{*|0}(s_j^*)$ of the nonseparable model in Lemma 2 if*

- (i.) $\mathbf{A} = \mathbf{U}\mathbf{D}/\sqrt{n}$, where \mathbf{U} and \mathbf{D} are defined through the SVD decomposition of $\mathbf{Y}(\mathbf{s}^{\mathcal{D}})$.
- (ii.) $v_i(\cdot)$ is the realization of independent mean zero Gaussian noises with the same variance.
- (iii.) $\sigma_0^2 = 0$.

3.1 Combining noises to weight functions

The nonseparable model (6) assumes a shared noise parameter σ_0^2 , which is typically very restrictive. We generalize the model by assuming different noise parameters as follows

$$\begin{aligned}\mathbf{Y}(s) &= \mathbf{A}\tilde{\mathbf{v}}(s) + \boldsymbol{\epsilon}_0, \\ \tilde{v}_i(\cdot) &= v_i(\cdot) + \epsilon_i, \quad i = 1, \dots, K,\end{aligned}\tag{11}$$

with $\boldsymbol{\epsilon}_0 \sim N(0, \sigma_0^2 \mathbf{I}_K)$ for any $s \in \mathcal{S}$, each weight function $v_i(\cdot)$ being assumed the same as the previous independent GaSP in (7) and ϵ_i being an independent zero-mean Gaussian noise with variance τ_i . We still assume $\mathbf{A} = \mathbf{U}\mathbf{D}/\sqrt{n}$ where \mathbf{U} and \mathbf{D} are defined through the SVD decomposition of $\mathbf{Y}(\mathbf{s}^{\mathcal{D}})$. An equivalent model of (11) is that each $\tilde{v}_i(\cdot)$ follows a zero-mean GaSP with noise

$$\tilde{v}_i(\cdot) \sim \text{GaSP}(0, \sigma_i^2 \tilde{c}_i(\cdot, \cdot)),\tag{12}$$

for $i = 1, \dots, K$, with the covariance

$$\sigma_i^2 \tilde{c}_i(s_a, s_b) = \sigma_i^2 (c_i(s_a, s_b) + \eta_i \mathbf{1}_{a=b}),$$

where $\eta_i = \tau_i/\sigma_i^2$ is the nugget-variance ratio and $c_i(\cdot, \cdot)$ is defined in (5) with a fixed ν_i and an unknown range parameter γ_i , for $i = 1, \dots, K$.

Replacing \mathbf{R}_i with $\tilde{\mathbf{R}}_i = \mathbf{R}_i + \eta_i \mathbf{I}_n$ in Lemma 1, the marginal likelihood of $\mathbf{Y}(\mathbf{s}^{\mathcal{D}})$ can be

written as a product of K independent multivariate normal densities,

$$p(\mathbf{Y}(\mathbf{s}^{\mathcal{D}}) | \sigma_{1:K}^2, \eta_{1:K}, \gamma_{1:K}) = |\mathbf{A}_v^T \mathbf{A}_v|^{-1/2} \prod_{i=1}^K p_{MN}(\hat{\mathbf{v}}_i(\mathbf{s}^{\mathcal{D}}); \mathbf{0}, \sigma_i^2 \tilde{\mathbf{R}}_i + \sigma_0^2 (\mathbf{a}_i^T \mathbf{a}_i)^{-1} \mathbf{I}_n), \quad (13)$$

where $\hat{\mathbf{v}}_i(\mathbf{s}^{\mathcal{D}})$ is the transpose of the i^{th} row of $\hat{\mathbf{v}}(\mathbf{s}^{\mathcal{D}}) = (\mathbf{A}^T \mathbf{A})^{-1} \mathbf{A}^T \mathbf{Y}(\mathbf{s}^{\mathcal{D}})$. The marginal likelihood in (10) is a special case of the marginal likelihood in (13) when $\eta_i = 0$ for $i = 1, \dots, K$. Note that the above model is not identifiable between η_1, \dots, η_K , and σ_0^2 . In the following, we simply constrain $\sigma_0^2 = 0$ to avoid the potential identifiability issue.

The predictive distributions at unobserved CpG sites are given in the following Lemma 3. The proof is essentially the same as Lemma 2, by replacing \mathbf{R}_i with $\tilde{\mathbf{R}}_i$ and setting $\sigma_0^2 = 0$.

Lemma 3. *We assume the same conditions as Lemma 1 and $\sigma_0 = 0$ for model (11).*

1. For every s_j^* ,

$$\mathbf{Y}(s_j^*) | \mathbf{Y}(\mathbf{s}^{\mathcal{D}}), \sigma_{1:K}^2, \eta_{1:K}, \gamma_{1:K} \sim MN\left(\tilde{\boldsymbol{\mu}}(s_j^*), \tilde{\boldsymbol{\Sigma}}(s_j^*)\right),$$

where $\tilde{\boldsymbol{\mu}}(s_j^*) = \mathbf{A} \tilde{\mathbf{v}}(s_j^*)$ and $\tilde{\boldsymbol{\Sigma}}(s_j^*) = \mathbf{A} \tilde{\mathbf{D}}(s_j^*) \mathbf{A}^T$, with $\tilde{\mathbf{v}}^*(s_j^*) = (\tilde{v}_1^*(s_j^*), \dots, \tilde{v}_K^*(s_j^*))^T$ and $\tilde{v}_i^*(s_j^*) = \mathbf{r}_i^T(s_j^*) \tilde{\mathbf{R}}_i^{-1} \hat{\mathbf{v}}_i(\mathbf{s}^{\mathcal{D}})$, $\tilde{\mathbf{D}}(s_j^*) = \text{diag}(\sigma_1^2 \tilde{c}_1^*(s_j^*), \dots, \sigma_K^2 \tilde{c}_K^*(s_j^*))$, $\tilde{c}_i^*(s_j^*) = \tilde{c}_i(s_j^*, s_j^*) - \mathbf{r}_i^T(s_j^*) \tilde{\mathbf{R}}_i^{-1} \mathbf{r}_i(s_j^*)$ and $\tilde{\mathbf{R}}_i = \mathbf{R}_i + \eta_i \mathbf{I}_n$.

2. Denote $\tilde{\boldsymbol{\mu}}(s_j^*) = (\tilde{\boldsymbol{\mu}}_0^T(s_j^*), \tilde{\boldsymbol{\mu}}_*^T(s_j^*))^T$ and $\tilde{\boldsymbol{\Sigma}}(s_j^*) = \begin{pmatrix} \tilde{\boldsymbol{\Sigma}}_{00}(s_j^*) & \tilde{\boldsymbol{\Sigma}}_{0*}(s_j^*) \\ \tilde{\boldsymbol{\Sigma}}_{*0}(s_j^*) & \tilde{\boldsymbol{\Sigma}}_{**}(s_j^*) \end{pmatrix}$. For every s_j^* ,

the predictive distribution of $\mathbf{y}^*(s_j^*)$ follows

$$\mathbf{y}^*(s_j^*) | \mathbf{y}(\mathbf{s}^{\mathcal{D}}), \mathbf{y}(\mathbf{s}^*), \mathbf{y}^*(\mathbf{s}^{\mathcal{D}}), \sigma_{1:K}^2, \eta_{1:K}, \gamma_{1:K} \sim MN\left(\tilde{\boldsymbol{\mu}}_{*|0}(s_j^*), \tilde{\boldsymbol{\Sigma}}_{*|0}(s_j^*)\right),$$

where $\tilde{\boldsymbol{\mu}}_{*|0}(s_j^*) = \tilde{\boldsymbol{\mu}}_*(s_j^*) + \tilde{\boldsymbol{\Sigma}}_{*0}(s_j^*) \tilde{\boldsymbol{\Sigma}}_{00}^{-1}(s_j^*) (\mathbf{y}(s_j^*) - \tilde{\boldsymbol{\mu}}_0(s_j^*))$,

and $\tilde{\boldsymbol{\Sigma}}_{*|0}(s_j^*) = \tilde{\boldsymbol{\Sigma}}_{**}(s_j^*) - \tilde{\boldsymbol{\Sigma}}_{*0}(s_j^*) \tilde{\boldsymbol{\Sigma}}_{00}^{-1}(s_j^*) \tilde{\boldsymbol{\Sigma}}_{0*}(s_j^*)$.

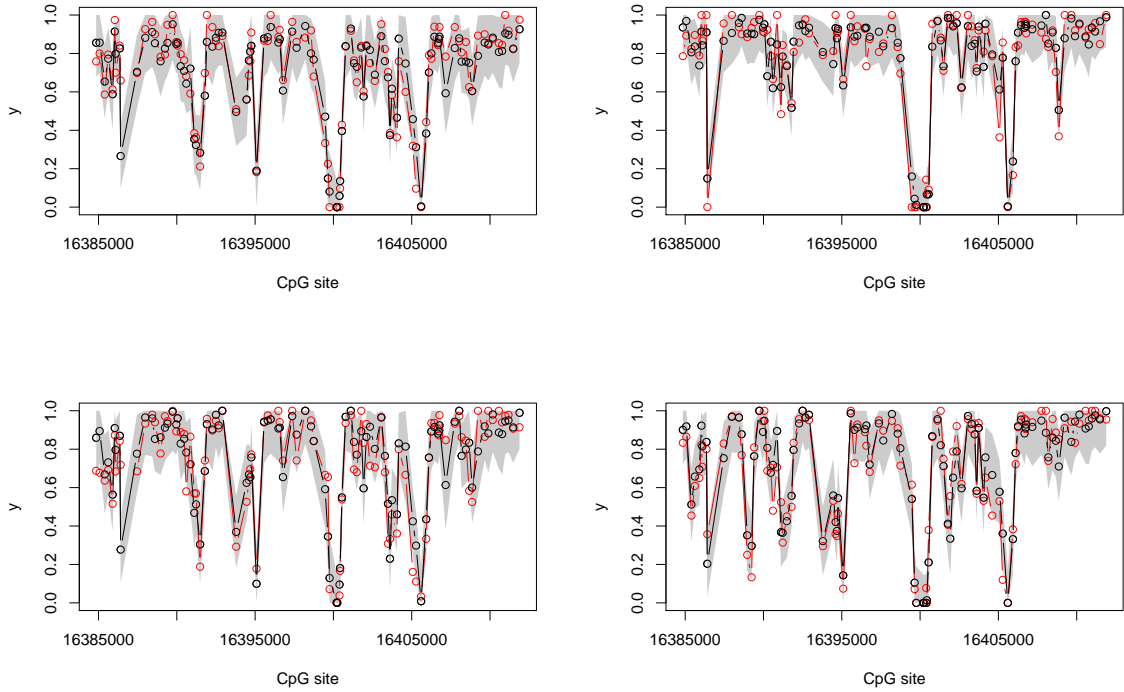


Figure 2: The held-out methylation levels (red circles) and prediction of methylation levels (black circles) by the nonseparable GaSP model for randomly selected 4 samples at 100 CpG sites. The 95% posterior predictive interval is dashed as the shaded area.

Figure 2 plots the predicted methylation levels as the black circles at 100 held-out CpG sites for 4 samples by $\tilde{\mu}_{*|0}(\cdot)$ in Lemma 3, with the examined methylation levels marked as the red circles. 95% posterior predictive credible interval for $\mathbf{y}^*(\mathbf{x}^*)$ is dashed as the shaded area. As shown in Figure 2, large uncertainties exist across different CpG sites and different samples. Therefore, only utilizing the information of nearby CpG sites or the correlations between samples might be too restrictive to predict accurately. Incorporating different sources of uncertainty is, thus, the key for modeling such complicated data. The prediction by the nonseparable GaSP model captures the pattern of the methylation levels reasonably well, with an adequate length of predictive 95% confidence interval, shown as the shaded area. A more detailed comparison between the nonseparable GaSP model and some

other computational feasible alternatives are given in Section 5.

3.2 Combing feature data

To impute the methylation levels, some site-specific features such as genomic position, DNA sequence properties, cis-regulatory element, can be used as covariates in a regression model. Incorporating regressors/covariates is less studied in the nonseparable GaSP model. In this section, we discuss a way to jointly model the site-specific features and output.

Let $\mathbf{X}(s)_{[q \times 1]}$ be features at site s (including the intercept). Consider an extended model

$$\mathbf{Y}^e(s) = \mathbf{A}^e \tilde{\mathbf{v}}(s) + \boldsymbol{\epsilon}_0, \quad (14)$$

for every $s \in \mathcal{S}$, where $\mathbf{Y}^e(s) = (\mathbf{X}^T(s); \mathbf{Y}^T(s))^T$, the weight $\tilde{\mathbf{v}}(\cdot)$ is defined the same as in (12), and $\boldsymbol{\epsilon}_0 \sim \mathcal{MN}(0, \sigma_0^2 \mathbf{I}_{K+q})$. Let $\mathbf{X}(\mathbf{s}^{\mathcal{D}})_{[q \times n]}$ be the features at sites $\mathbf{s}^{\mathcal{D}}$ and $\mathbf{Y}^e(\mathbf{s}^{\mathcal{D}}) = (\mathbf{X}^T(\mathbf{s}^{\mathcal{D}}); \mathbf{Y}^T(\mathbf{s}^{\mathcal{D}}))^T$. The extended basis matrix $\mathbf{A}^e = \mathbf{U}^e \mathbf{D}^e / \sqrt{n}$, where \mathbf{U}^e and \mathbf{D}^e are still defined through the SVD decomposition $\mathbf{Y}^e(\mathbf{s}^{\mathcal{D}}) = \mathbf{U}^e \mathbf{D}^e \mathbf{V}^e$. The predictive distribution of the model (14) can be obtained similarly to Lemma 3.

The connection among regression model, the separable GaSP model, and the nonseparable GaSP model shown in the previous section still holds. Let \mathbf{Z}^e follow a matrix normal distribution with mean zero and covariance $\boldsymbol{\Sigma}^e \otimes \boldsymbol{\Lambda}$, where $\boldsymbol{\Sigma}^e = \begin{pmatrix} \boldsymbol{\Sigma}_{00}^e & \boldsymbol{\Sigma}_{0*}^e \\ \boldsymbol{\Sigma}_{*0}^e & \boldsymbol{\Sigma}_{**}^e \end{pmatrix}$ is a $(q+K) \times (q+K)$ covariance matrix. The separable model is a special case of the nonseparable GaSP model (14) specified in Remark 1. The prediction by the regression model (2) with covariates $\mathbf{H}_i(s_j) = (\mathbf{X}^T(s_j); \mathbf{y}^T(s_j))^T$ is also a special case of the extended nonseparable GaSP model specified in Remark 2.

4 Computational strategy of the nonseparable GaSP model

The computation of the conditional distribution in Lemma 2 and Lemma 3 requires to compute the inverse of \mathbf{R}_i , each with $O(n^3)$ operations. In addition, the storage of \mathbf{R}_i requires $O(n^2)$, making the implementation impractical when n is large. We introduce a computationally efficient algorithm, based on the connection between the Gaussian random field and Gaussian Markov random field (GMRF). The idea can be traced back to Whittle (1954, 1963), where the Matérn covariance was shown to have a Markov structure, and more recently discussed in Hartikainen and Sarkka (2010); Särkkä and Hartikainen (2012). We first review these ideas.

Consider a continuous time auto-regressive model with order p , defined by a stochastic differential equation (SDE),

$$c_p f^{(p)}(s) + c_{p-1} f^{(p-1)}(s) + \dots + c_0 f(s) = b_0 z(s), \quad (15)$$

where $f^{(l)}(s)$ is the l^{th} derivative of $f(s)$ and $z(s)$ is the standard Gaussian white noise process defined on $s \in \mathbb{R}$. Here we set $c_p = 1$ to avoid the nonidentifiability issue. The spectral density of equation (15) is

$$S_{\mathbb{R}}(t) = \frac{b_0^2}{|C(2\pi it)|^2}, \quad (16)$$

where i is the imaginary number, and the operator $C(\cdot)$ is defined by $C(z) = \sum_{l=0}^p c_l z^l$. The form of the above spectral density is

$$S_{\mathbb{R}}(t) = \frac{\text{constant}}{\text{polynomial in } t^2}, \quad (17)$$

which is a rational functional form. It has been shown in Whittle (1954, 1963) that the spectral density of GaSP with the Matérn covariance is

$$S_{Mat}(t) \propto \frac{1}{(\lambda^2 + t^2)^{(\nu+1/2)}}, \quad (18)$$

where $\lambda = \frac{\sqrt{2\nu}}{\gamma}$ with the range parameter γ and the roughness parameter ν . It is easy to see that the spectral density in (18) also follows a rational functional form. Wiener-Khinchin theorem states that the stationary covariance function of the process is given by the inverse Fourier transformation of the spectral density, meaning that the covariance function is uniquely determined (Wiener, 1930; Rasmussen, 2006).

The benefits of using the GMRF representation is that the computational operations of the prediction is linear to the number of sites, discussed in the following subsection.

4.1 The computation by continuous time stochastic process

Here we assume the Matérn kernel with $\nu = 5/2$ as an example for the demonstration purpose, which has the following expression

$$c(d) = \left(1 + \frac{\sqrt{5}d}{\gamma} + \frac{5d^2}{3\gamma^2}\right) \exp\left(-\frac{\sqrt{5}d}{\gamma}\right), \quad (19)$$

with $d = |s_a - s_b|$ for any $s_a, s_b \in \mathcal{S}$. The computational advantages introduced in this subsection hold for Matérn kernel with $\nu = (2m + 1)/2$ for all $m \in \mathbb{N}$.

As shown in (13), the likelihood of $\mathbf{Y}(\mathbf{s}^{\mathcal{S}})$ in model (11) with $\sigma_0^2 = 0$ can be written in terms of $\tilde{\mathbf{v}}(\mathbf{s}^{\mathcal{S}}) = (\mathbf{A}^T \mathbf{A})^{-1} \mathbf{A}^T \mathbf{Y}(\mathbf{s}^{\mathcal{S}})$. We thus focus on discussing the likelihood of $\tilde{\mathbf{v}}(\mathbf{s}^{\mathcal{S}})$.

The nonseparable GaSP model in (11) with $\sigma_0^2 = 0$ can be represented as

$$\begin{aligned}\tilde{v}_i(\cdot) &= f_i(\cdot) + \epsilon_i, \\ f_i(\cdot) &\sim \text{GaSP}(0, \sigma_i^2 c_i(\cdot, \cdot)), \\ \epsilon_i &\sim \mathcal{N}(0, \tau_i),\end{aligned}\tag{20}$$

where $\tau_i = \sigma_i^2 \eta_i$, for $1 \leq i \leq K$. Denote $\boldsymbol{\theta}_i(s) := (f_i(s), f_i^{(1)}(s), f_i^{(2)}(s))^T$, where $f_i^{(l)}(s)$ is the l^{th} derivative of $f_i(s)$ with regard to s , $l = 1, 2$. As discussed above, for each $i = 1, \dots, K$, Gaussian stochastic process with Matérn correlation function defined in (19) can be written as an SDE

$$\frac{d\boldsymbol{\theta}_i(s)}{ds} = \mathbf{J}_i \boldsymbol{\theta}_i(s) + \mathbf{L} z_i(s),$$

or in a matrix form

$$\frac{d}{ds} \begin{pmatrix} f_i(s) \\ f_i^{(1)}(s) \\ f_i^{(2)}(s) \end{pmatrix} = \begin{pmatrix} 0 & 1 & 0 \\ 0 & 0 & 1 \\ -\lambda_i^3 & -\lambda_i^2 & -3\lambda_i \end{pmatrix} \begin{pmatrix} f_i(s) \\ f_i^{(1)}(s) \\ f_i^{(2)}(s) \end{pmatrix} + \begin{pmatrix} 0 \\ 0 \\ 1 \end{pmatrix} z_i(s),$$

where $z_i(s)$ is a zero-mean Gaussian white noise process with variance σ_i^2 and $\lambda_i = \sqrt{2\nu_i}/\gamma_i$. Denote $q_i = \frac{16}{3}\sigma_i^2\lambda_i^5$ and $\mathbf{F} = (1, 0, 0)$. The solution of the above SDE can be represented

explicitly as a continuous state space model (Hartikainen and Sarkka, 2010),

$$\begin{aligned}
\tilde{v}_i(s_{j+1}) &= \mathbf{F}\boldsymbol{\theta}_i(s_{j+1}) + \epsilon_i, \\
\boldsymbol{\theta}_i(s_{j+1}) &= \mathbf{G}_i(s_j)\boldsymbol{\theta}_i(s_j) + \mathbf{W}_i(s_j) \\
\mathbf{G}_i(s_j) &= e^{\mathbf{J}_i(s_{j+1}-s_j)} \\
\mathbf{W}_i(s_j) &\sim N(0, \mathbf{Q}_i(s_j)) \\
\mathbf{Q}_i(s_j) &= \int_0^{s_{j+1}-s_j} e^{\mathbf{J}_i t} \mathbf{L} q_i \mathbf{L}^T e^{\mathbf{J}_i^T t} dt,
\end{aligned} \tag{21}$$

for $j = 1, \dots, n - 1$. The stationary distribution of $\boldsymbol{\theta}_i$, is

$$\boldsymbol{\theta}_i(s_0) \sim MN(0, \mathbf{Q}_i(s_0)),$$

with $\mathbf{Q}_i(s_0) = \int_0^\infty e^{\mathbf{J}_i t} \mathbf{L} q_i \mathbf{L}^T e^{\mathbf{J}_i^T t} dt$. We derive all $\mathbf{G}_i(s_j)$, $\mathbf{Q}_i(s_j)$, $\mathbf{Q}_i(s_0)$, and the joint likelihood of $\boldsymbol{\theta}_i$, shown in Appendix B.

With the above setup, the posterior for $\boldsymbol{\theta}_i(s)$, $i = 1, \dots, K$, can be computed by a forward filtering and backward sampling/smoothing (FFBS) algorithm (West and Harrison, 1997; Petris et al., 2009), which only requires $O(n)$ computational operations, a lot smaller than $O(n^3)$ operations in the direct computation of the GaSP model. The prediction at \mathbf{s}^* also only requires linear computational operations to the number of sites, so the total computational operations are only $O(N)$ altogether. Furthermore, $\boldsymbol{\theta}_i(s)$ can be explicitly marginalized out for all s instead of the posterior sampling, discussed in Section 4.2.

Figure 3 compares the posterior means of $\tilde{\mathbf{v}}_i(\mathbf{s}^*) \mid \tilde{\mathbf{v}}_i(\mathbf{s}^\mathcal{D})$ by the FFBS algorithm and direct computation of GaSP for some s_j^* with a given set of parameters. Since they are the same quantities computed in two different ways, the difference only depends on the machine precision, which is extremely small. The main advantage of our method is that all summary statistics of interest, such as the posterior predictive mean and variance, as well

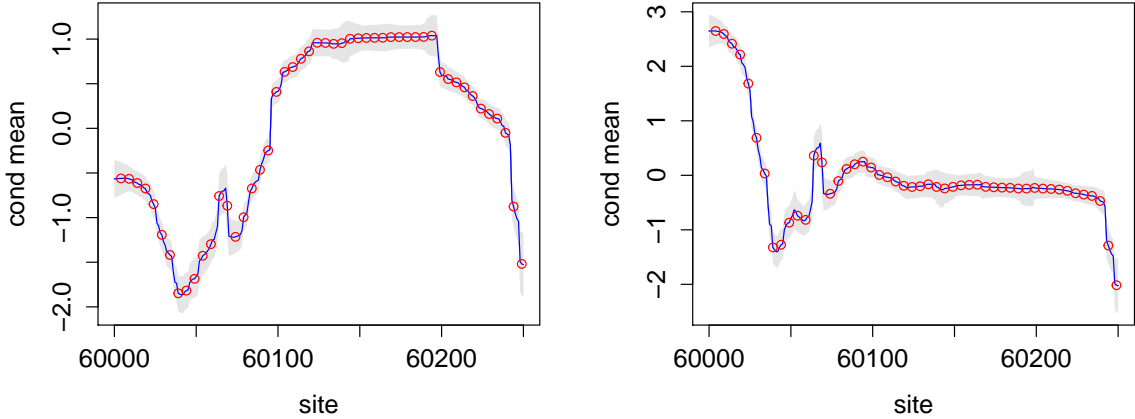


Figure 3: Comparison of the predictive mean by the direct computation of the GaSP likelihood and the FFBS algorithm for two weights functions. The blue curves are the posterior mean of $\tilde{\mathbf{v}}_i(\mathbf{s}^*)|\tilde{\mathbf{v}}_i(\mathbf{s}^{\mathcal{D}})$ by equation (21) and the shaded area is the 95% posterior predictive interval of the mean function at a small region for $i = 1$ (left panel) and $i = 2$ (right panel), for a given set of parameters $(\sigma_i^2, \gamma_i, \tau_i)$. The red dots are the posterior mean $\tilde{\mathbf{v}}_i(\mathbf{s}_j^*)|\tilde{\mathbf{v}}_i(\mathbf{s}^{\mathcal{D}})$ of 50 s_j^* at the same region with the same set of parameters by the direct computation for the GaSP model. The root of mean square errors (RMSE) between the blue curves and red circles at these 50 s_j^* are 2.04×10^{-13} and 2.41×10^{-12} for the left panel and right panel respectively.

as the marginal likelihood can be computed exactly.

The computational time between them, however, differs significantly. As shown in Figure 4, the computation by the FFBS algorithm is a lot more efficient than the direct evaluation of the likelihood, which requires $O(n^3)$ for matrix inversion. For instance, when $n = 5,000$, evaluating the likelihood by the FFBS algorithm only takes around 0.1 second on a laptop, while the direct computation takes around 60 seconds.

Note when $\nu_i = 5/2$, the Matérn covariance matrix in (19) and its inversion are both dense $n \times n$ matrices with rank n . However, the covariance matrix of the latent states is sparse shown in the Appendix B. The algorithm relies on the augmented variables $\boldsymbol{\theta}_i(s) = (f_i(s), f_i^{(1)}(s), f_i^{(2)}(s))^T$ for the fast computation, and these augmented variables can be marginalized out iteratively. This holds for all Matérn classes when $\nu_i = (2m + 1)/2$, with

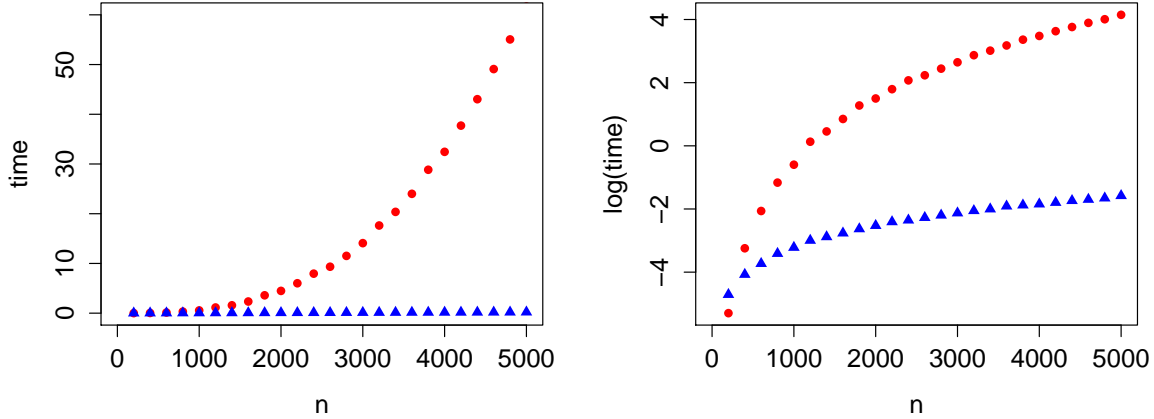


Figure 4: Comparison of computational time in seconds for one evaluation of the likelihood with the normal scale (left panel) and log scale (right panel). The red dot represents the computational time by the direct computation and blue solid triangle is by the FFBS algorithm.

$m \in \mathbb{N}$. When m gets larger, the computation of $G_i(s_j)$ and $Q_i(s_j)$ in Equation (21) becomes more time-consuming, as both of them are $m \times m$ matrix. Therefore, the approximation would be needed when Matérn covariance functions with large m are used.

4.2 Parameter estimation and prediction

The most computationally intensive part of the FFBS algorithm is to sample $3Kn$ latent states $\boldsymbol{\theta}_i(s_j)$ for $i = 1, \dots, K$ and $j = 1, \dots, n$. Fortunately, one can avoid it by marginalizing out the latent states explicitly,

$$p(\tilde{\mathbf{v}}(\mathbf{s}^{\mathcal{D}}) | \boldsymbol{\sigma}_{1:K}^2, \boldsymbol{\tau}_{1:K}, \boldsymbol{\gamma}_{1:K}) = \prod_{i=1}^K \left\{ p(\tilde{v}_i(s_1^{\mathcal{D}}) | \sigma_i^2, \tau_i, \gamma_i) \prod_{j=2}^n p(\tilde{v}_i(s_j^{\mathcal{D}}) | \tilde{v}_i(\mathbf{s}_{1:j-1}^{\mathcal{D}}), \sigma_i, \tau_i, \gamma_i) \right\},$$

each term of which follows a normal distribution given in the one-step look ahead prediction in the FFBS algorithm (West and Harrison, 1997; Petris et al., 2009). The marginal likelihood $p(\tilde{\mathbf{v}}(\mathbf{s}^{\mathcal{D}}) | \gamma_i, \eta_i, \sigma_i^2)$ can also be computed with linear computational operations in terms of n ,

allowing us to evaluate the likelihood without making an approximation.

To complete the model, we assume the prior as follows,

$$\pi(\boldsymbol{\sigma}_{1:K}^2, \boldsymbol{\tau}_{1:K}, \boldsymbol{\gamma}_{1:K}) \propto \prod_{i=1}^K \frac{\pi(\tau_i, \gamma_i)}{\sigma_i^2}. \quad (22)$$

Denote $\zeta_i = 1/\gamma_i$, $\eta_i = \tau_i/\sigma_i^2$. We use the jointly robust prior for computational efficiency (Gu, 2016),

$$\pi(\zeta_i, \eta_i) \propto (C_i \zeta_i + \eta_i)^{a_i} \exp(-b_i(C_i \zeta_i + \eta_i)), \quad (23)$$

for $i = 1, \dots, K$, where C_i , a_i and b_i are prior parameters. This prior approximates the reference prior in tail rates and is computationally efficient with a closed-form expression of the mean and variance. For the prior parameter, we use the default choice $a = 1/2$, $b = 1$, and $C_l = |\mathcal{S}|/n$, where $|\mathcal{S}|$ is the volume of the space \mathcal{S} .

One can use the Markov chain Monte Carlo (MCMC) algorithm to sample the parameters from their posterior distributions. Here we estimate the parameters by the posterior mode,

$$(\hat{\zeta}_i, \hat{\eta}_i) = \underset{\zeta_i, \eta_i}{\operatorname{argmax}} \{p(\tilde{\mathbf{v}}(\mathbf{s}^{\mathcal{D}})|\zeta_i, \eta_i)\pi(\zeta_i, \eta_i)\}. \quad (24)$$

The posterior mode of the variance parameters is $\hat{\sigma}_i^2 = S_i^2/(n+1)$ with $S_i^2 = \tilde{\mathbf{v}}_i^T(\mathbf{s}^{\mathcal{D}})\tilde{\mathbf{R}}_i^{-1}\tilde{\mathbf{v}}_i^T(\mathbf{s}^{\mathcal{D}})$. The posterior mean and the MLE of σ_i^2 are $S_i^2/(n-1)$ and S_i^2/n respectively. When n is large, these estimations are almost the same. This is of course an approximation to the full Bayesian inference. However, such approximation is different from approximating the likelihood, as the algorithm is already scalable to the problem with large n .

After obtaining the estimates $(\hat{\zeta}_i, \hat{\eta}_i, \hat{\sigma}_i^2)$ for each i , $i = 1, \dots, K$, one can plug in these estimates in Lemma 3 for the predictive distribution.

5 Numerical comparison

We evaluate the performance of the nonseparable GaSP model and compare to several alternative methods: two linear regression strategies (by site in (1) and by sample in (2)), nearest neighborhood method (using only the observed methylation level that is located closest to the unobserved site for prediction), and two regression tree strategies using the random forest algorithm (Liaw and Wiener, 2002).

Denote $y_i^*(s_j^*)$, $1 \leq i \leq k^*$ and $1 \leq j \leq n^*$ as the held-out methylation levels of the i^{th} sample at the j^{th} CpG site. The criteria we employ are

$$\begin{aligned}
 RMSE &= \sqrt{\frac{\sum_{i=1}^{k^*} \sum_{j=1}^{n^*} (\hat{y}_i^*(s_j^*) - y_i^*(s_j^*))^2}{k^*n^*}}, \\
 P_{CI}(95\%) &= \frac{1}{k^*n^*} \sum_{i=1}^{k^*} \sum_{j=1}^{n^*} 1\{y_i^*(s_j^*) \in CI_{ij}(95\%)\}, \\
 L_{CI}(95\%) &= \frac{1}{k^*n^*} \sum_{i=1}^{k^*} \sum_{j=1}^{n^*} \text{length}\{CI_{ij}(95\%)\},
 \end{aligned}$$

where $\hat{y}_i^*(s_j^*)$ is the predicted held-out methylation level of the i^{th} sample at the j^{th} CpG site; $CI_{ij}(95\%)$ is the 95% posterior credible interval; and $\text{length}\{CI_{ij}(95\%)\}$ is the length of the 95% posterior credible interval. An effective method is expected to have small out-of-sample RMSE, $P_{CI}(95\%)$ being close to nominal 95% level, and small $L_{CI}(95\%)$. In Zhang et al. (2015), a CpG site is defined to be methylated if more than 50% of the probes are methylated, and the accuracy rate of a method is defined by the proportion of the correct predictions of CpG sites being methylated or not. We also show the predictive accuracy rate by the nonseparable GaSP model and its competitors in the following numerical results.

5.1 Real dataset 1: WGBS data

We first compare the out-of-sample prediction of different methods using the criteria discussed above for roughly 10^6 methylation levels in the WGBS dataset. In this dataset, 24 samples are available in total and we randomly select $k^* = 4$ samples, whose methylation levels are partially observed (with certain proportion being held out), while the methylation levels of the rest of the samples are fully observed. We consider four scenarios, in which 25%, 50%, 75%, and 90% of the methylation levels of these 4 samples are held out as the test dataset. The methylation levels of each sample are centered and the mean is added back for prediction in the GaSP model (Higdon et al., 2008). We estimate the range and nugget parameters using equation (24) and rely on Lemma 3 for combining different sources of information in prediction.

As shown in Table 1, the nonseparable GaSP model has the smallest out-of-sample RMSE, making it the most accurate in out-of-sample prediction in all scenarios. For instance, when 50% of CpG sites are held out, the nonseparable GaSP method improves the RMSE by at least 15% compared to any other methods we considered. The gain is from integrating the correlations between CpG sites and between samples through a coherent statistical model, while the other models only utilize partial information. For example, the methods in rows 2 to 4 only exploit the site-wise correlation by assuming the observations are independent across different samples at each CpG site, while the methods in rows 5 to 6 only exploit the correlation between samples.

When more and more data are held-out as the test data, the correlation between nearby observed methylation levels gets smaller as the average distance between two sites with observed methylation levels gets larger, making it harder for prediction. Yet the nonseparable GaSP model still results in the smallest RMSE, which is around 0.089 and 0.096, when 75% and 90% of CpG sites are held out respectively.

Furthermore, the nonseparable GaSP model produces 95% credible interval that covers

25% held-out CpG sites	RMSE	$P_{CI}(95\%)$	$L_{CI}(95\%)$	Accuracy
Nonseparable GaSP	0.084	0.955	0.282	0.971
Nearest neighborhood	0.150	/	/	0.944
Linear model by site	0.108	0.916	0.280	0.963
Random forest by site	0.097	/	/	0.966
Linear model by sample	0.100	0.941	0.306	0.963
Random forest by sample	0.095	/	/	0.965
50% held-out CpG sites	RMSE	$P_{CI}(95\%)$	$L_{CI}(95\%)$	Accuracy
Nonseparable GaSP	0.085	0.961	0.300	0.970
Nearest neighborhood	0.147	/	/	0.943
Linear model by site	0.100	0.913	0.261	0.966
Random forest by site	0.103	/	/	0.964
Linear model by sample	0.100	0.941	0.308	0.962
Random forest by sample	0.101	/	/	0.963
75% held-out CpG sites	RMSE	$P_{CI}(95\%)$	$L_{CI}(95\%)$	Accuracy
Nonseparable GaSP	0.089	0.961	0.309	0.968
Nearest neighborhood	0.166	/	/	0.934
Linear model by site	0.106	0.910	0.274	0.963
Random forest by site	0.108	/	/	0.962
Linear model by sample	0.100	0.941	0.308	0.962
Random forest by sample	0.097	/	/	0.964
90% held-out CpG sites	RMSE	$P_{CI}(95\%)$	$L_{CI}(95\%)$	Accuracy
Nonseparable GaSP	0.096	0.941	0.296	0.966
Nearest neighborhood	0.166	/	/	0.934
Linear model by site	0.114	0.908	0.289	0.959
Random forest by site	0.114	/	/	0.957
Linear model by sample	0.100	0.941	0.308	0.962
Random forest by sample	0.098	/	/	0.963

Table 1: Comparison of different methods for the WGBS data. From the upper to the lower, 25%, 50%, 75% and 90% of the first million methylation levels of $k^* = 4$ samples are held out for testing, respectively.

approximately 95% of the held-out outcomes, with the comparatively short length of credible interval. In contrast, two linear regression models are over-confident, as the coverages are all below the nominal 95% level. This is not surprising, because the independence assumption by the linear models (either between sites or between samples) makes the likelihood too concentrated. Consequently, the predictive interval by the linear model is typically too

narrow to cover the held-out samples as it claims, while the likelihood of the nonseparable GaSP model describes the complicated patterns of correlation better, thereby presenting an adequate predictive credible interval.

The nonseparable GaSP also leads to around 97% accuracy in predicting whether a CpG site is methylated or not (equivalently predicting whether more than half of the probes are methylated in the held-out CpG sites), which is also the highest compared to all other methods. Note the differences between the nonseparable model and other methods are small, as around 90% of the CpG sites are methylated in this dataset, and thus a benchmark estimator could achieve at least 90% accuracy in prediction. However, in certain important regions such as CGI shore regions (Zhang et al., 2015) in which half of CpG sites are not methylated, the differences are much bigger.

We need to mention that the computation of the nonseparable GaSP model relies heavily on the fast and exact computation algorithm discussed in Section 4. Since the number of methylation levels is at the size of a million in one chromosome in one sample, direct computation of the GaSP model is infeasible. Among all models, the most time consuming model is the random forest. The random forest by sample performs the second best, which is roughly 2% to 4% better than the linear model by sample, and much better than the linear model and random forest by site. This matches our intuition that the correlation between samples is stronger than the correlations between sites, especially when a large proportion of the methylation levels are unobserved.

5.2 Real dataset 2: Methylation450 data

In this section, we study the numerical performance of all the methods for the Methy450K dataset (Zhang et al., 2015). In this dataset, the methylation levels of 100 samples are recorded. For the purpose of comparison, 20% of the CpG sites of $k^* = 50$ samples are held out. We do not hold out more sites in this dataset, because the Methy450K data only

	RMSE	$PCI(95\%)$	$L_{CI}(95\%)$	Accuracy
Nonseparable GaSP	0.030	0.972	0.122	0.991
Nearest neighborhood	0.150	/	/	0.944
Linear model by site	0.034	0.945	0.099	0.990
Random forest by site	0.034	/	/	0.990
Linear model by sample	0.031	0.957	0.106	0.990
Random forest by sample	0.031	/	/	0.990

Table 2: Comparison of different methods for the Methylation450K data. 20% CpG sites of the $k^* = 50$ people are held out for testing.

contain about 2% Methylation levels in the WGBS whole sequencing dataset.

In Table 2, the prediction based on the nonseparable GaSP model has the lowest RMSE, though the differences to the other methods are smaller compared with the ones in the previous WGBS data since the CpG sites are sparse in this data set, resulting in the small site-wise correlation. Modeling both the correlation by site and by sample in the nonseparable GaSP model improves around 10% and 3% in terms of the RMSE compared to the models only exploiting correlation by site and by sample, respectively.

5.3 Comparison to approximation methods by blocks

In this subsection, we compare our exact and fast computation of the nonseparable GaSP model with a straightforward approximation, in which the long sequence is divided into small blocks and GaSP models are built independently in each block. Assume the data are divided into M blocks, each with n_0 inputs (where $n = Mn_0$), the computational operations of which are then $O(Mn_0^3)$ instead of $O(n^3)$ for the inversion of the covariance matrix.

For illustration purposes, the data are divided into 100 batches and 200 CpG sites are used as the training data in each batch. We consider two scenarios, with 600 CpG sites and 66 CpG sites between these 200 CpG sites being selected as the test CpG sites in each batch, respectively. That means that roughly 75% and 25% of the data are held out. We

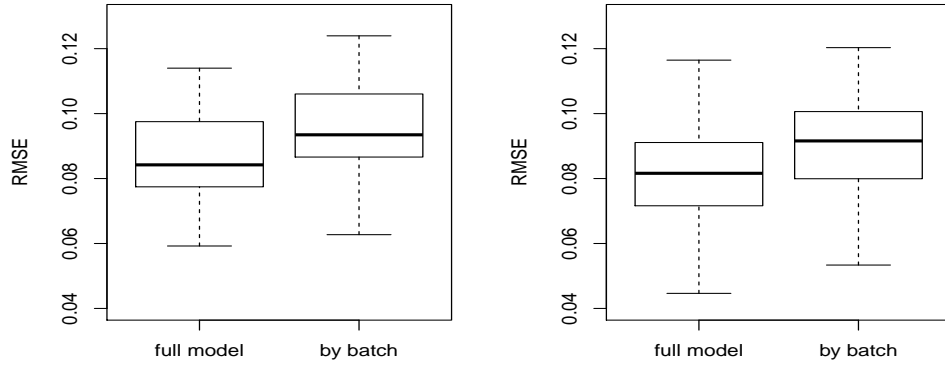


Figure 5: Boxplots of $RMSE_j$ for the test samples in batch j with 75% of CpG sites (left panel) and 25% of CpG sites (right panel) being held-out, respectively, $j = 1, \dots, 100$.

still assume the methylation levels for the first 20 samples are available at all CpG sites and 4 randomly selected samples are only partially observed. The total number of the test CpG sites is 240,000 and 26,400, respectively.

As shown in Table 3, the prediction by the nonseparable GaSP with the full model is about 10% better in terms of RMSE in both scenarios. This is further justified by Figure 5. One possible reason is that the boundary effect is large in the approximation method when we divide the data into batches. All these results suggest that simply approximating the likelihood by batch yields inferior predictive results than the nonseparable GaSP model with the full likelihood. Again, the implementation of the full model relies on the FFBS algorithm we discussed in Section 4.

6 Concluding remarks

This paper discusses modeling multiple functional data through Gaussian stochastic processes. We unify several different models, including the linear regression model and separable model, through a nonseparable GaSP framework. We provide a computationally efficient

25% held-out CpG sites	RMSE	$P_{CI}(95\%)$	$L_{CI}(95\%)$	Accuracy
Nonseparable GaSP full model	0.083	0.956	0.278	0.969
Nonseparable GaSP by batch	0.091	0.923	0.258	0.966
75% held-out CpG sites	RMSE	$P_{CI}(95\%)$	$L_{CI}(95\%)$	Accuracy
Nonseparable GaSP full model	0.087	0.963	0.305	0.968
Nonseparable GaSP by batch	0.096	0.934	0.283	0.966

Table 3: Comparison of different methods in terms of out of sample prediction for WGBS data with 25% and 75% CpG sites are held out for testing.

algorithm that can evaluate the likelihoods with linear operations in number of inputs without approximation. Numerical results suggest that the nonseparable GaSP model performs the best compared to the alternative models we considered. Because different sources of correlations are incorporated into a coherent model, the likelihood is more sensible than other models with independence assumptions between samples or between sites, making the prediction more accurate.

Several interesting future topics are worth exploring from both the computational and modeling perspectives. The achievement in computation is limited, in a sense that the input of the GaSP model (CpG site) is only 1 dimensional. It remains to be an issue to generalize this computational method for the case with multi-dimensional inputs. Some recent progresses of this direction are introduced in Lindgren et al. (2011)), where the GaSP with a Matérn covariance can be represented by stochastic partial differential equations. Second, the unification of different models relies on the choice of SVD basis, which is data dependent. It is more satisfying if we are able to take into account the uncertainty by choosing a basis through a multi-resolution statistical model. Furthermore, for the methylation datasets, the range of outcomes is $[0, 1]$ with lots of 0 and 1 in the data. A more appropriate likelihood such as a mixture of a point process with masses at 0 and 1 and a GaSP might improve the prediction.

Appendix A

proof of Lemma 1. Because $\mathbf{A} = \mathbf{U}\mathbf{D}/\sqrt{n}$, $\mathbf{A}(\mathbf{A}^T\mathbf{A})^{-1}\mathbf{A}^T = \mathbf{I}_K$. The likelihood is

$$\begin{aligned}\mathcal{L}(\mathbf{Y}_v(\mathbf{s}^{\mathcal{D}})|\mathbf{v}_v(\mathbf{s}^{\mathcal{D}}), \sigma_0^2) &= (2\pi\sigma_0^2)^{-nK/2} \exp\left(-\frac{(\mathbf{Y}_v(\mathbf{s}^{\mathcal{D}}) - \mathbf{A}_v\mathbf{v}_v(\mathbf{s}^{\mathcal{D}}))^T (\mathbf{Y}_v(\mathbf{s}^{\mathcal{D}}) - \mathbf{A}_v\mathbf{v}_v(\mathbf{s}^{\mathcal{D}}))}{2\sigma_0^2}\right) \\ &= (2\pi\sigma_0^2)^{-nK/2} \exp\left(-\frac{(\hat{\mathbf{v}}_v(\mathbf{s}^{\mathcal{D}}) - \mathbf{v}_v(\mathbf{s}^{\mathcal{D}}))^T \mathbf{A}_v^T \mathbf{A}_v (\hat{\mathbf{v}}_v(\mathbf{s}^{\mathcal{D}}) - \mathbf{v}_v(\mathbf{s}^{\mathcal{D}}))}{2\sigma_0^2}\right),\end{aligned}$$

where $\hat{\mathbf{v}}_v(\mathbf{s}^{\mathcal{D}}) = (\mathbf{A}_v^T \mathbf{A}_v)^{-1} \mathbf{A}_v^T \mathbf{Y}_v(\mathbf{s}^{\mathcal{D}})$. $\mathbf{A}_v^T \mathbf{A}_v$ is a diagonal matrix because

$$\mathbf{A}_v^T \mathbf{A}_v = \begin{pmatrix} (\mathbf{I}_n \otimes \mathbf{a}_1)^T (\mathbf{I}_n \otimes \mathbf{a}_1) & (\mathbf{I}_n \otimes \mathbf{a}_1)^T (\mathbf{I}_n \otimes \mathbf{a}_2) & \dots & (\mathbf{I}_n \otimes \mathbf{a}_1)^T (\mathbf{I}_n \otimes \mathbf{a}_K) \\ (\mathbf{I}_n \otimes \mathbf{a}_2)^T (\mathbf{I}_n \otimes \mathbf{a}_1) & (\mathbf{I}_n \otimes \mathbf{a}_2)^T (\mathbf{I}_n \otimes \mathbf{a}_2) & \dots & (\mathbf{I}_n \otimes \mathbf{a}_2)^T (\mathbf{I}_n \otimes \mathbf{a}_K) \\ \dots & \dots & \dots & \dots \\ (\mathbf{I}_n \otimes \mathbf{a}_K)^T (\mathbf{I}_n \otimes \mathbf{a}_1) & (\mathbf{I}_n \otimes \mathbf{a}_K)^T (\mathbf{I}_n \otimes \mathbf{a}_2) & \dots & (\mathbf{I}_n \otimes \mathbf{a}_K)^T (\mathbf{I}_n \otimes \mathbf{a}_K) \end{pmatrix},$$

with $(\mathbf{I}_n \otimes \mathbf{a}_i)^T (\mathbf{I}_n \otimes \mathbf{a}_i) = (\mathbf{I}_n^T \otimes \mathbf{a}_i^T) (\mathbf{I}_n \otimes \mathbf{a}_i) = (\mathbf{I}_n^T \mathbf{I}_n) \otimes (\mathbf{a}_i^T \mathbf{a}_i)$ and $(\mathbf{I}_n \otimes \mathbf{a}_i)^T (\mathbf{I}_n \otimes \mathbf{a}_j) = (\mathbf{I}_n^T \mathbf{I}_n) \otimes (\mathbf{a}_i^T \mathbf{a}_j) = \mathbf{O}$, where \mathbf{O} is a matrix with each element being 0. Marginalizing out $\mathbf{v}_v(\mathbf{s}^{\mathcal{D}})$, one has

$$\begin{aligned}& \mathcal{L}(\mathbf{Y}_v(\mathbf{s}^{\mathcal{D}})|\sigma_0^2, \sigma_1^2, \dots, \sigma_K^2, \mathbf{R}_1, \dots, \mathbf{R}_K) \\ &= \int \mathcal{L}(\mathbf{Y}_v(\mathbf{s}^{\mathcal{D}})|\mathbf{v}_v(\mathbf{s}^{\mathcal{D}}), \sigma_0^2) p(\mathbf{v}_v(\mathbf{s}^{\mathcal{D}})|\sigma_1^2, \dots, \sigma_K^2, \mathbf{R}_1, \dots, \mathbf{R}_K) d\mathbf{v}_v(\mathbf{s}^{\mathcal{D}}) \\ &= |\mathbf{A}_v^T \mathbf{A}_v|^{-1/2} (2\pi)^{-nK/2} |\boldsymbol{\Sigma}_v + \sigma_0^2 (\mathbf{A}_v^T \mathbf{A}_v)^{-1}|^{-1/2} \exp\left(-\frac{1}{2} \hat{\mathbf{v}}_v(\mathbf{s}^{\mathcal{D}})^T (\boldsymbol{\Sigma}_v + \sigma_0^2 (\mathbf{A}_v^T \mathbf{A}_v)^{-1})^{-1} \hat{\mathbf{v}}_v(\mathbf{s}^{\mathcal{D}})\right) \\ &= |\mathbf{A}_v^T \mathbf{A}_v|^{-1/2} \times \\ & \quad \prod_{i=1}^K \left\{ (2\pi)^{-n/2} |\sigma_i^2 \mathbf{R}_i + \sigma_0^2 (\mathbf{a}_i^T \mathbf{a}_i)^{-1} \mathbf{I}_n|^{-1/2} \exp\left(-\frac{1}{2} \hat{\mathbf{v}}_i(\mathbf{s}^{\mathcal{D}})^T (\sigma_i^2 \mathbf{R}_i + \sigma_0^2 (\mathbf{a}_i^T \mathbf{a}_i)^{-1} \mathbf{I}_n)^{-1} \hat{\mathbf{v}}_i(\mathbf{s}^{\mathcal{D}})\right) \right\}.\end{aligned}$$

The last row follows from the fact that $\hat{\mathbf{v}}_i(\mathbf{s}^{\mathcal{D}})^T$ is the i^{th} row of the matrix $\hat{\mathbf{v}}(\mathbf{s}^{\mathcal{D}})$. \square

proof of Lemma 2. Denote $\mathbf{Y}(\mathbf{s}^{\mathcal{D}}; s_j^*) := [\mathbf{Y}(\mathbf{s}^{\mathcal{D}}); Y(s_j^*)]$ and $\mathbf{v}(\mathbf{s}^{\mathcal{D}}; s_j^*) := [\mathbf{v}(\mathbf{s}^{\mathcal{D}}); v(s_j^*)]$. Both are $k \times (n+1)$ matrices.

Vectorizing the output $\mathbf{Y}_v(\mathbf{s}^{\mathcal{D}}, s_j^*) := \text{vec}(\mathbf{Y}(\mathbf{s}^{\mathcal{D}}, s_j^*))$, a $K \times (n+1)$ vector, and $\mathbf{v}_v(\mathbf{s}^{\mathcal{D}}) := \text{vec}(\mathbf{v}(\mathbf{s}^{\mathcal{D}})^T)$, we can write model (6) as,

$$\mathbf{Y}_v(\mathbf{s}^{\mathcal{D}}, s_j^*) = \mathbf{A}_v \mathbf{v}_v(\mathbf{s}^{\mathcal{D}}, s_j^*) + \boldsymbol{\epsilon},$$

where $\boldsymbol{\epsilon} \sim N(0, \sigma_0^2 \mathbf{I}_{(n+1)K})$. Similar to the proof of Lemma 1, one has

$$L(\mathbf{Y}_v(\mathbf{s}^{\mathcal{D}}, s_j^*) | \boldsymbol{\sigma}_{0:K}^2, \boldsymbol{\gamma}_{1:K}) = |\mathbf{A}_v^T \mathbf{A}_v|^{-1/2} \prod_{i=1}^K p_{MN}(\hat{\mathbf{v}}_i(\mathbf{s}^{\mathcal{D}}, s_j^*); \mathbf{0}, \sigma_i^2 \boldsymbol{\Lambda}_i + \sigma_0^2 (\mathbf{a}_i^T \mathbf{a}_i)^{-1} \mathbf{I}_{n+1}),$$

where $\hat{\mathbf{v}}_i(\mathbf{s}^{\mathcal{D}}, s_j^*)$ is the transpose of the i^{th} row of the $\hat{\mathbf{v}}(\mathbf{s}^{\mathcal{D}}, s_j^*) := (\mathbf{A}^T \mathbf{A})^{-1} \mathbf{A}^T \mathbf{Y}(\mathbf{s}^{\mathcal{D}}, s_j^*)$ and

$$\boldsymbol{\Lambda}_i = \begin{pmatrix} \mathbf{R}_i & \mathbf{r}_i(s_j^*) \\ \mathbf{r}_i^T(s_j^*) & c_i(s_j^*, s_j^*) \end{pmatrix}. \text{ One has}$$

$$\hat{v}_i(s_j^*) | \hat{\mathbf{v}}_i(\mathbf{s}^{\mathcal{D}}), \boldsymbol{\sigma}_0^2, \sigma_i^2, \boldsymbol{\gamma}_i \sim MN(\hat{v}_i^*(s_j^*), \sigma_i^2 c^*(s_j^*) + \sigma_0^2 (\mathbf{a}_i^T \mathbf{a}_i)^{-1}), \quad (25)$$

with $\hat{v}_i^*(s_j^*) = \mathbf{r}_i^T(s_j^*) (\mathbf{R}_i + \frac{\sigma_0^2 (\mathbf{a}_i^T \mathbf{a}_i)^{-1}}{\sigma_i^2} \mathbf{I}_n)^{-1} \hat{\mathbf{v}}_i(\mathbf{s}^{\mathcal{D}})$ and $c_i^*(s_j^*) = c_i(s_j^*, s_j^*) - \mathbf{r}_i^T(s_j^*) (\mathbf{R}_i + \frac{\sigma_0^2 (\mathbf{a}_i^T \mathbf{a}_i)^{-1}}{\sigma_i^2} \mathbf{I}_n)^{-1} \mathbf{r}_i(s_j^*)$.

Note $\mathbf{A}(\mathbf{A}^T \mathbf{A})^{-1} \mathbf{A}^T = \mathbf{I}_K$. One has $\mathbf{Y}(s_j^*) = \mathbf{A} \hat{\mathbf{v}}(s_j^*)$ and $\mathbf{Y}(s^{\mathcal{D}}) = \mathbf{A} \hat{\mathbf{v}}(s^{\mathcal{D}})$. Applying the properties of multivariate normal distribution to (25) leads to the results.

□

Appendix B

The quantities of continuous state space model representation in (21) are shown in this Appendix. The following results hold for every subscript i , $1 \leq i \leq k$, so the subscript is

dropped for simplicity. Denote $d_j = |s_j - s_{j-1}|$.

$$e^{\mathbf{J}d_j} = \frac{e^{-\lambda d_j}}{2} \begin{pmatrix} \lambda^2 d_j^2 + 2\lambda + 2 & 2(\lambda d_j^2 + d_j) & d_j^2 \\ -\lambda^3 d_j^2 & -2(\lambda^2 d_j^2 - \lambda d_j - 1) & 2d_j - \lambda d_j^2 \\ \lambda^4 d_j^2 - 2\lambda^3 d_j & 2(\lambda^3 d_j^2 - 3\lambda^2 d_j) & \lambda^2 d_j^2 - 4\lambda d_j + 2 \end{pmatrix}$$

$$\mathbf{Q}(s_j) = \frac{4\sigma^2 \lambda^5}{3} \begin{pmatrix} Q_{1,1}(s_j) & Q_{1,2}(s_j) & Q_{1,3}(s_j) \\ Q_{2,1}(s_j) & Q_{2,2}(s_j) & Q_{2,3}(s_j) \\ Q_{3,1}(s_j) & Q_{3,2}(s_j) & Q_{3,3}(s_j) \end{pmatrix},$$

with

$$Q_{1,1}(s_j) = \frac{e^{-2\lambda d_j} (3 + 6\lambda d_j + 6\lambda^2 d_j^2 + 4\lambda^3 d_j^3 + 2\lambda^4 d_j^4) - 3}{-4\lambda^5},$$

$$Q_{1,2}(s_j) = Q_{2,1}(s_j) = \frac{e^{-2\lambda d_j} d_j^4}{2},$$

$$Q_{1,3}(s_j) = Q_{3,1}(s_j) = \frac{e^{-2\lambda d_j} (1 + 2\lambda d_j + 2\lambda^2 d_j^2 + 4\lambda^3 d_j^3 - 2\lambda^4 d_j^4) - 1}{4\lambda^3},$$

$$Q_{2,2}(s_j) = \frac{e^{-2\lambda d_j} (1 + 2\lambda d_j + 2\lambda^2 d_j^2 - 4\lambda^3 d_j^3 + 2\lambda^4 d_j^4) - 1}{-4\lambda^3},$$

$$Q_{2,3}(s_j) = Q_{3,2}(s_j) = \frac{e^{-2\lambda d_j} d_j^2 (4 - 4\lambda d_j + \lambda^2 d_j^2)}{2},$$

$$Q_{3,3}(s_j) = \frac{e^{-2\lambda d_j} (-3 + 10\lambda^2 d_j^2 - 22\lambda^2 d_j^2 + 12\lambda^2 d_j^2 - 2\lambda^4 d_j^4) + 3}{4\lambda},$$

and

$$\mathbf{Q}(s_0) = \begin{pmatrix} \sigma^2 & 1 & -\sigma^2 \lambda^2 / 3 \\ 0 & \sigma^2 \lambda^2 / 3 & 1 \\ -\sigma^2 \lambda^2 / 3 & 0 & \sigma^2 \lambda^4 \end{pmatrix}.$$

The joint distribution of $\boldsymbol{\theta}(s_{0:n})$ is given by

$$\begin{pmatrix} \boldsymbol{\theta}(s_0) \\ \boldsymbol{\theta}(s_1) \\ \boldsymbol{\theta}(s_2) \\ \dots \\ \boldsymbol{\theta}(s_n) \end{pmatrix} \sim MN \left(\begin{pmatrix} 0 \\ 0 \\ 0 \\ \dots \\ 0 \end{pmatrix}, \begin{pmatrix} \mathbf{Q}(s_0)^{-1} & & & & \\ -\mathbf{G}^T(s_1)\mathbf{Q}(s_1)^{-1}\mathbf{G}(s_1) & \mathbf{Q}^{-1}(s_1) & & & \\ -\mathbf{G}^T(s_2)\mathbf{Q}(s_2)^{-1}\mathbf{G}(s_2) & & \mathbf{Q}^{-1}(s_2) & & \\ & & & \dots & \\ & & & & \mathbf{Q}^{-1}(s_n) \end{pmatrix} \right)^{-1}.$$

References

- Alvarez, M. A. and Lawrence, N. D. (2011). Computationally efficient convolved multiple output Gaussian processes. *Journal of Machine Learning Research*, 12(5):1459–1500.
- Álvarez, M. A., Rosasco, L., and Lawrence, N. D. (2011). Kernels for vector-valued functions: a review. *arXiv preprint arXiv:1106.6251*.
- Banerjee, S., Carlin, B. P., and Gelfand, A. E. (2014). *Hierarchical modeling and analysis for spatial data*. Crc Press.
- Banerjee, S., Gelfand, A. E., Finley, A. O., and Sang, H. (2008). Gaussian predictive process models for large spatial data sets. *Journal of the Royal Statistical Society: Series B (Statistical Methodology)*, 70(4):825–848.
- Bayarri, M. J., Berger, J. O., Calder, E. S., Dalbey, K., Lunagomez, S., Patra, A. K., Pitman, E. B., Spillerh, E. T., and Wolperti, R. L. (2009). Using statistical and computer models to quantify volcanic hazards. *Technometrics*, 51:402–413.
- Bayarri, M. J., Berger, J. O., Paulo, R., Sacks, J., Cafeo, J. A., Cavendish, J., Lin, C.-H., and Tu, J. (2007). A framework for validation of computer models. *Technometrics*, 49(2):138–154.
- Conti, S. and O’Hagan, A. (2010). Bayesian emulation of complex multi-output and dynamic computer models. *Journal of statistical planning and inference*, 140(3):640–651.

- Cressie, N. and Johannesson, G. (2008). Fixed rank kriging for very large spatial data sets. *Journal of the Royal Statistical Society: Series B (Statistical Methodology)*, 70(1):209–226.
- Das, P. M. and Singal, R. (2004). DNA methylation and cancer. *Journal of Clinical Oncology*, 22(22):4632–4642.
- Eckhardt, F., Lewin, J., Cortese, R., Rakyan, V. K., Attwood, J., Burger, M., Burton, J., Cox, T. V., Davies, R., Down, T. A., et al. (2006). DNA methylation profiling of human chromosomes 6, 20 and 22. *Nature genetics*, 38(12):1378–1385.
- Eidsvik, J., Shaby, B. A., Reich, B. J., Wheeler, M., and Niemi, J. (2013). Estimation and prediction in spatial models with block composite likelihoods. *Journal of Computational and Graphical Statistics*, 23(2):295–315.
- Furrer, R., Genton, M. G., and Nychka, D. (2012). Covariance tapering for interpolation of large spatial datasets. *Journal of Computational and Graphical Statistics*.
- Gelfand, A. E., Diggle, P., Guttorp, P., and Fuentes, M. (2010). *Handbook of spatial statistics*. CRC Press.
- Gelfand, A. E., Schmidt, A. M., Banerjee, S., and Sirmans, C. (2004). Nonstationary multivariate process modeling through spatially varying coregionalization. *Test*, 13(2):263–312.
- Gu, M. (2016). *Robust uncertainty quantification and scalable computation for computer models with massive output*. PhD thesis, Duke University.
- Gu, M., Wang, X., and Berger, J. O. (2017+). Robust Gaussian stochastic process emulation. *The Annals of Statistics*.
- Hartikainen, J. and Sarkka, S. (2010). Kalman filtering and smoothing solutions to temporal gaussian process regression models. In *Machine Learning for Signal Processing (MLSP), 2010 IEEE International Workshop on*, pages 379–384. IEEE.

- Higdon, D. et al. (2002). Space and space-time modeling using process convolutions. *Quantitative methods for current environmental issues*, 3754.
- Higdon, D., Gattiker, J., Williams, B., and Rightley, M. (2008). Computer model calibration using high-dimensional output. *Journal of the American Statistical Association*, 103(482):570–583.
- Kaufman, C. G., Bingham, D., Habib, S., Heitmann, K., and Frieman, J. A. (2011). Efficient emulators of computer experiments using compactly supported correlation functions, with an application to cosmology. *The Annals of Applied Statistics*, 5(4):2470–2492.
- Kaufman, C. G., Schervish, M. J., and Nychka, D. W. (2008). Covariance tapering for likelihood-based estimation in large spatial data sets. *Journal of the American Statistical Association*, 103(484):1545–1555.
- Liaw, A. and Wiener, M. (2002). Classification and regression by randomforest. *R news*, 2(3):18–22.
- Lindgren, F., Rue, H., and Lindström, J. (2011). An explicit link between gaussian fields and gaussian markov random fields: the stochastic partial differential equation approach. *Journal of the Royal Statistical Society: Series B (Statistical Methodology)*, 73(4):423–498.
- Petris, G., Petrone, S., and Campagnoli, P. (2009). *Dynamic linear models*. Springer.
- Rasmussen, C. E. (2006). *Gaussian processes for machine learning*. MIT Press.
- Rue, H., Martino, S., and Chopin, N. (2009). Approximate Bayesian inference for latent Gaussian models by using integrated nested Laplace approximations. *Journal of the royal statistical society: Series b (statistical methodology)*, 71(2):319–392.
- Sacks, J., Welch, W. J., Mitchell, T. J., Wynn, H. P., et al. (1989). Design and analysis of computer experiments. *Statistical science*, 4(4):409–423.

- Särkkä, S. and Hartikainen, J. (2012). Infinite-dimensional kalman filtering approach to spatio-temporal gaussian process regression. In *International Conference on Artificial Intelligence and Statistics*, pages 993–1001.
- Scarano, M. I., Strazzullo, M., Matarazzo, M. R., and D’Esposito, M. (2005). DNA methylation 40 years later: Its role in human health and disease. *Journal of cellular physiology*, 204(1):21–35.
- Sun, Y., Li, B., and Genton, M. G. (2012). *Geostatistics for large datasets*. Springer.
- Wang, H. and West, M. (2009). Bayesian analysis of matrix normal graphical models. *Biometrika*, 96(4):821–834.
- West, M. and Harrison, P. J. (1997). *Bayesian Forecasting & Dynamic Models*. Springer Verlag, 2nd edition.
- Whittle, P. (1954). On stationary processes in the plane. *Biometrika*, pages 434–449.
- Whittle, P. (1963). Stochastic process in several dimensions. *Bulletin of the International Statistical Institute*, 40(2):974–994.
- Wiener, N. (1930). Generalized harmonic analysis. *Acta mathematica*, 55(1):117–258.
- Xu, Y. and Ji, Y. (2014). A latent Gaussian process model with application to monitoring clinical trials. *arXiv preprint arXiv:1403.7853*.
- Zhang, W., Spector, T. D., Deloukas, P., Bell, J. T., and Engelhardt, B. E. (2015). Predicting genome-wide DNA methylation using methylation marks, genomic position, and DNA regulatory elements. *Genome biology*, 16(14):1–20.